ELSEVIER

Journal of Nuclear Materials 279 (2000) 335–343

journal of nuclear materials

www.elsevier.nl/locate/jnucmat

Effects of Sn and Nb on massive hydriding kinetics of Zr–XSn–YNb alloy

Y.-s. Kim [a,*], S.-k. Kim [a], J.-g. Bang [b], Y.-h. Jung [b]

[a] *Department of Nuclear Engineering, Hanyang University, 17 Haengdang-Dong, Sungdong-Ku, Seoul 133-791, South Korea*
[b] *Korea Atomic Energy Research Institute, 150 Dukjin-Dong, Yusong-Ku, Taejon 305-353, South Korea*

Received 7 May 1999; accepted 11 November 1999

Abstract

Kinetic studies on the massive hydriding of Zr–0.4Nb–*X*Sn ($X = 0.5, 0.8, 1.5, 2.0$) and Zr–0.8Sn–*Y*Nb ($Y = 0.2, 0.4, 0.8, 1.0$) ternary alloys are carried out at 400°C under atmospheric pressure by in situ weight gain measurements with thermo-gravimetric apparatus (TGA) and transmission electron microscope/energy dispersive X-ray spectrometer (TEM/EDX) analysis. It is confirmed that the hydriding kinetics follow a linear rate law after incubation time. It is found that the hydriding reaction rate decreases with increasing Sn content up to 1.5% and then sharply increases in the case of Zr–0.4Nb–*X*Sn while it steadily increases with Nb content in the case of Zr–0.8Sn–*Y*Nb. The rate does not seem to be affected by the grain size in the *X*Sn alloys, but is influenced in the *Y*Nb alloys. TEM/EDX analysis shows that there is no strong relationship between the intermetallic precipitates and the kinetic rate in the Zr–*X*Sn–*Y*Nb alloy system. It is revealed in this study that the solubility limit of Sn in the Zr–0.4Nb–*X*Sn ternary system becomes higher than that in the Zr–Sn binary system. On the other hand, the Nb solubility limit remains unchanged in the Zr–0.8Sn–*Y*Nb ternary system. Optimized compositions in the Zr–*X*Sn–*Y*Nb ternary alloy are suggested to be about 1.5% Sn and as low Nb as possible in order to minimize hydrogen uptake.

1. Introduction

Since the late 1970s, nuclear fuel performance and reliability have significantly improved by virtue of resolving many of the early fuel failure problems such as primary hydriding and pellet cladding interaction (PCI). Accordingly, high fuel duties with high burn-up and extended fuel cycle operation have been demanded for economical nuclear power generation, resulting in an increased fuel peaking factor and decreased operation margin. In addition, recent water chemistry changes demand even more from fuel cladding.

Due to the high demand, plant surveillance programs have been conducted for fuel design improvement lately, which show that Zircaloy cladding corrosion is the limiting factor for the high duty operation of PWR fuels. Therefore, research and development of new or improved Zr alloy cladding are being extensively carried out worldwide, primarily focusing on the enhancement of corrosion resistance and mechanical integrity.

Recently, several reports have been published suggesting that hydride precipitation at the metal/oxide interface may be one of the main causes of the accelerated corrosion of Zircaloy-4 cladding at high burn-up [1–3]. Thus, it seems to be essential in the developmental stage to take into consideration the effects of alloying elements not only on the corrosion resistance, but also on the hydriding behaviors. In the present study, the effects of Sn and Nb, two prime candidate alloying elements, on the massive hydriding behaviors of zirconium alloys, are examined with Zr–*X*Sn–*Y*Nb ternary alloys.

2. Experimental

Thermo-gravimetric apparatus (TGA) experiments under atmospheric pressure are carried out at 400°C to measure the weight gain by hydrogen absorption

* Corresponding author. Tel.: +82-2-2290-0467; fax: +82-2-2281-5131.
E-mail address: yongskim@numater.hanyang.ac.kr (Y.-s. Kim).

0022-3115/00/$ - see front matter
PII: S0022-3115(99)00281-0

reaction. A schematic diagram of the apparatus is shown in Fig. 1. A specimen is suspended by a platinum wire connected to the quartz beam in the micro-balance weighting cell which is maintained at room temperature by circulating cooling water. The weighting cell and the reaction chamber are filled with helium gas prior to the actual experiments to prevent oxidation during heating to the reaction temperature. When the desired temperature of the reaction chamber is reached, hydrogen gas flow into the reaction chamber is initiated at the flow rate of 200 cm^3/min. Then, weight gain is continuously measured and recorded every 15 s by a data acquisition system connected to a personal computer. The experiment is terminated when sudden weight gain decrease caused by spalling of the embrittled specimen takes place. The sensitivity of the electro-microbalance system (model S3D-P, Satorius) is 1 μg and the purities of both the hydrogen and the helium gases are 99.999%.

The specimens used in this study are recrystallized Zr, Zr–0.4Nb–*X*Sn, and Zr–0.8Sn–*Y*Nb ternary alloy coupons (0.8 mm in thickness). They are cut to 1.0× 2.0 cm^2 (equivalent to ~1.1 g) thin plates with a diamond-wafered low speed saw, ground mechanically with 1500 grit SiC paper, pickled in a solution of 50% H_2O +

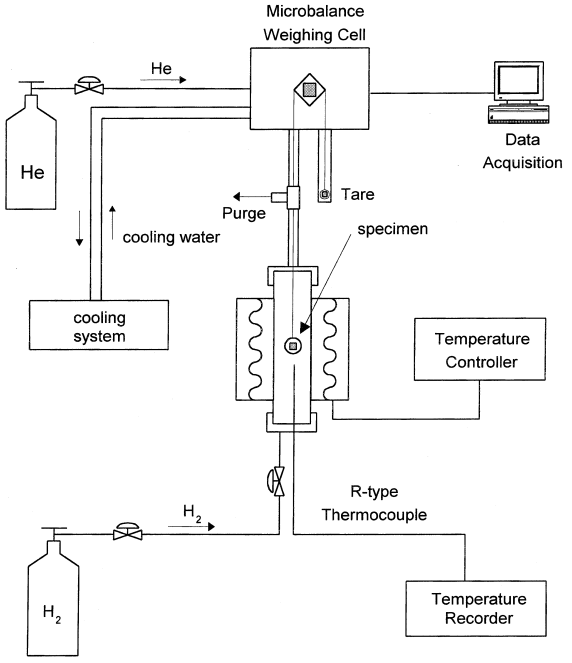

Fig. 1. A schematic diagram of TGA (thermo-gravimetric apparatus).

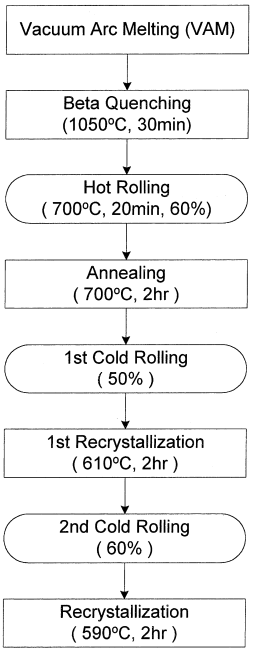

Fig. 2. Fabrication history of Zr, Zr–0.4Nb–*X*Sn and Zr–0.8Sn–*Y*Nb ternary alloys.

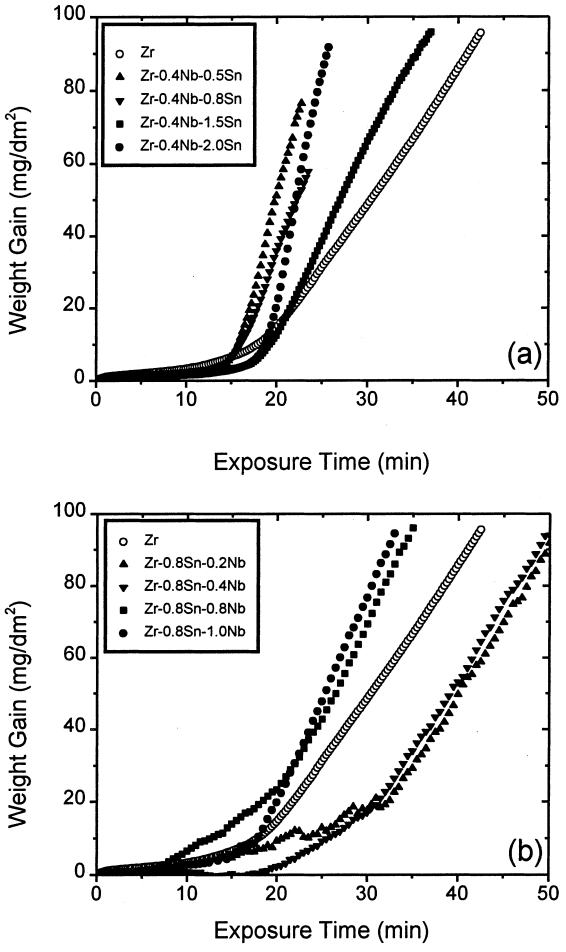

Fig. 3. Weight gain behaviors of ternary zirconium alloys with reaction time at 400°C: (a) Zr–0.4Nb–*X*Sn; (b) Zr–0.8Sn–*Y*Nb.

47% HNO_{3+} 3% HF for 3 min to remove pre-filmed surface oxide, and cleaned ultrasonically in acetone. The fabrication histories of the alloys are all identical (Fig. 2).

Transmission electron microscope/energy dispersive X-ray spectrometer (TEM/EDX) examinations are performed to analyze the precipitates in the alloys and their compositions quantitatively. TEM specimens are mechanically ground to 80 μm in thickness, punched into 3 mm diameter disks, and thinned in 90% methanol +10% perchloric acid with a jet-polishing at a voltage of 13 V at −45°C.

3. Results and discussion

3.1. Massive hydriding kinetic behaviors

Weight gain behaviors of Zr–0.4Nb–*X*Sn and Zr–0.8Sn–*Y*Nb ternary alloys by the hydrogen absorption are shown and compared in Fig. 3(a) and (b), respectively. As seen in the figures, rapid weight gain rates of the alloys are observed after the termination of incubation time which ranges from 5 to 20 min depending on the alloys. For reference, the weight gain of 1 mg in current experiments is equivalent to the hydrogen content of ~900 ppm.

It is well known that the incubation is attributed to the thin surface oxide film formed during prior heating, which is inevitable even under the vacuum condition of about 10^{-5} Pa [4]. The thin oxide film has been confirmed by the SEM/EDX analysis in the previous work [5]. The figure shows that once the massive hydriding initiates, the weight gains of the two alloys increase linearly with increasing reaction time. This linear kinetic behavior is demonstrated by the replotted plots in Figs. 4(a) and 5(a) after the beginning of the massive hydriding. The hydriding kinetics of the zirconium alloys is supported by a literature survey.

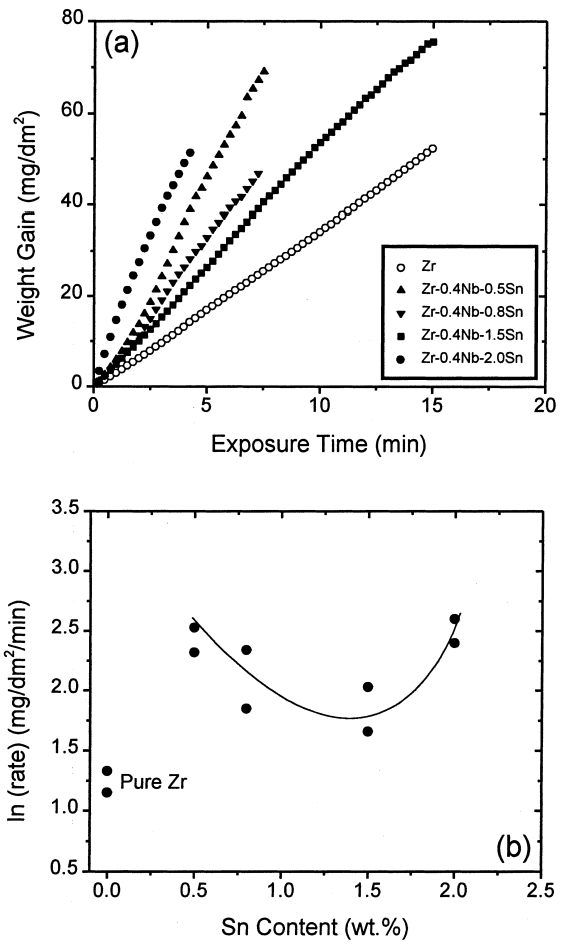

Fig. 4. (a) Weight gain behaviors of Zr–0.4Nb–*X*Sn alloys at 400° since the onset of massive hydriding. (b) Reaction rate constant vs. Sn content.

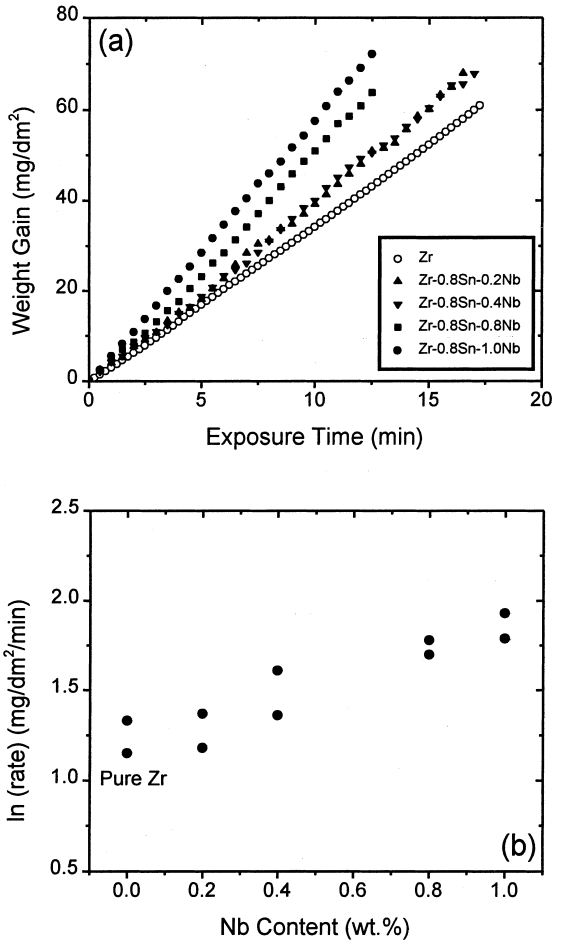

Fig. 5. (a) Weight gain behaviors of Zr–0.8Sn–*Y*Nb alloys at 400°C since the onset of massive hydriding. (b) Reaction rate constant vs. Nb content.

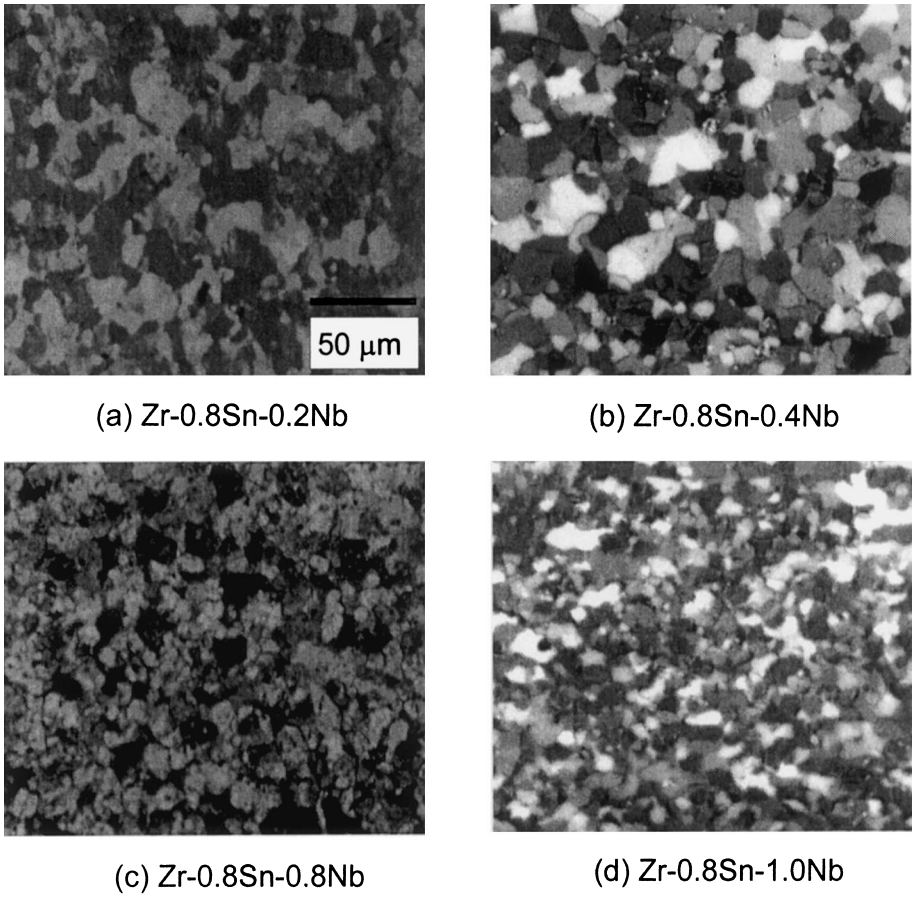

Fig. 6. Microstructure of Zr–0.4Nb–*X*Sn alloys.

Early researchers in around 1950 reported that the kinetics deviates from a linear rate law or appears to be following a parabolic law [6,7]. However, recent investigations with more sophisticated apparatus show that the kinetics follows a linear rate law and can deviate from the linearity as temperature goes down, especially down to 300°C [5,8,9]. In fact, it is known that the deviation is ascribed to the diffusion of hydrogen through Zr matrix since it becomes drastically slow as temperature decreases.

Based on the linear kinetics in Fig. 4(a), reaction rate constants for the hydriding reaction of Zr–0.4Nb–*X*Sn are derived as a function of Sn content and plotted in Fig. 4(b). The figure demonstrates that pure zirconium (less than 0.08% Fe, 0.03% Ni) has the lowest hydriding reaction rate and the rates of the alloys decrease with increasing Sn content up to 1.5%, and then increase quite sharply. In practice, the effect of Sn on hydrogen pick-up still remains controversial under the in-pile condition. Some claimed that hydrogen pick-up is accelerated with increasing Sn content [10], but others reported that it decreases with Sn [11].

In the mean time, derived hydriding rate constants of Zr–0.8Sn–*Y*Nb as a function of Nb content show that the reaction rate steadily increases with increasing Nb content (Fig. 5(b)). Unlike this result, it has been reported that Nb-containing alloys have low hydrogen pick-up fraction under the in-pile condition [12]. It seems to be inconsistent; however, it must be understood that the situation is quite different. The former is a case of direct hydriding reaction while the latter is a case of hydrogen pick-up which is a reaction of residual hydrogen atoms with Zr base metal through the oxide layer in the waterside corrosion.

3.2. Microscopic analysis using TEM/EDX

The kinetic behaviors can be affected by recrystallized grain size change, intermetallic precipitate formation, and hydrogen absorption by the alloying element itself. Therefore, in order to review and discuss the influential factors, microscopic analyses using TEM/EDX are performed. First, the microstructures of Zr–0.4Nb–*X*Sn and Zr–0.8Sn–*Y*Nb alloys are observed with an optical

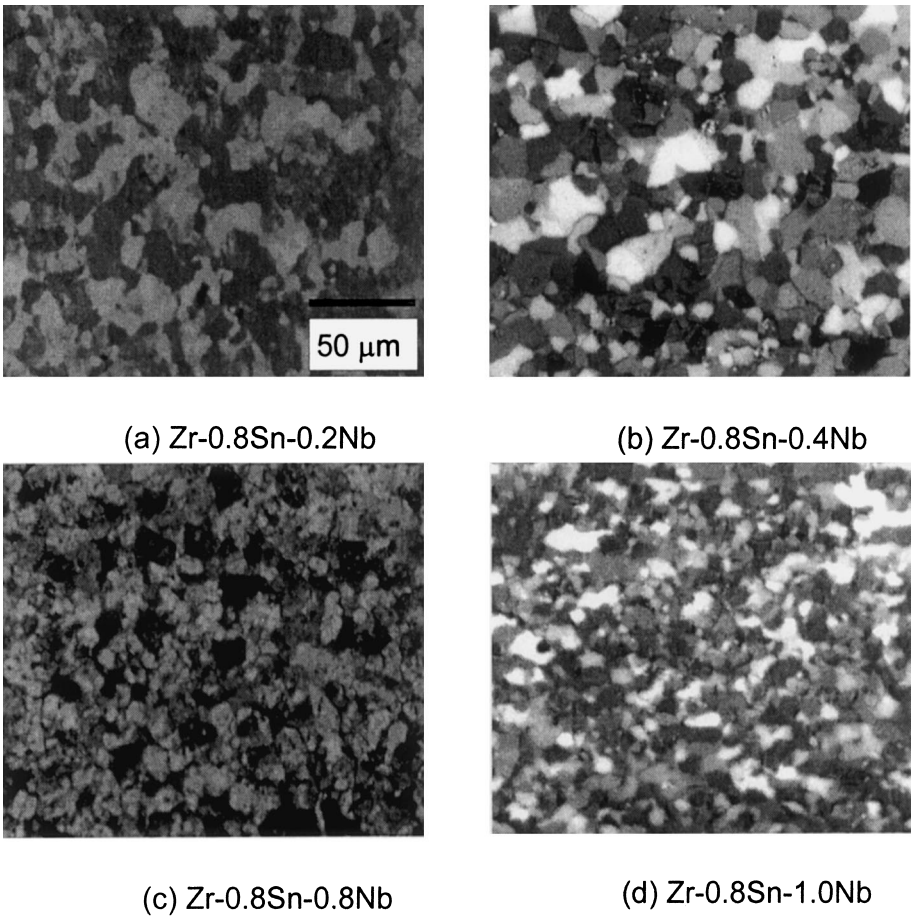

Fig. 7. Microstructure of Zr–0.8Sn–*Y*Nb alloys.

microscope. Figs. 6 and 7 show that the recrystallized grain sizes of both alloys decrease with the addition of a third element, Sn or Nb. In general, the decrease in grain size may be conducive to faster hydrogen absorption because it results in the increase of grain boundary area. As a matter of fact, Sn addition in Zr–0.4Nb–*X*Sn alloy decreases the hydriding reaction rate gradually, then raises it sharply when the content exceeds 1.5 wt%. However, Nb addition in Zr–0.8Sn–*Y*Nb alloy increases the hydriding reaction rate steadily. Therefore, it seems that this grain size change may not affect the kinetic rate in Zr–0.4Nb–*X*Sn alloy, but may influence that in Zr–0.8Sn–*Y*Nb alloy.

As is well-known, the intermetallic precipitates in the zirconium alloys play significant roles in the waterside corrosion of the fuel cladding [13–15]. Therefore, they may act as sites on the surface for accelerating the hydrogen absorption since the hydriding reaction is surface reaction-controlled. In general, the roles of the precipitates are closely related to the solubility limits, and their sizes and compositions. It is reported that the solubility limit of Sn in the binary is about 1.5% and that of Nb is 0.5% [16]. However, their solubility limits in the ternary alloy are not certain. Thus, in order to examine the formation and the sizes of the intermetallic compounds, TEM/EDX analyses for both alloys are carried out. Fig. 8(a) and (b) show that, in the cases of low Nb alloys, e.g., Zr–0.8Sn–0.2Nb and Zr–0.8Sn–0.4Nb, only a few precipitates are observed, which turn out to be Zr (Fe,Cr) and Zr_3(Fe,Cr)-type precipitates. Although Fe and Cr are impurity elements in the alloy, they can easily form compounds with Zr since the maximum solubilities of Fe and Cr in the Zr alloys are very low (120 ppm for iron at 820°C and 200 ppm for chromium at 860°C [17]). It is well-known that $Zr(Fe, Cr)_2$-type precipitates are typically observed in zircaloy-4 [18–20]. The compositions of Fe and Cr in the precipitates are analyzed to be 33.61 and 10.95% for Zr–0.8Sn–0.2Nb alloy and 19.11 and 5.02% for Zr–0.8Sn–0.4Nb alloy, respectively, by EDX attached to TEM. When Nb content exceeds 0.4 wt%, many precipitates are observed (Fig. 8(c) and (d)), which means that the

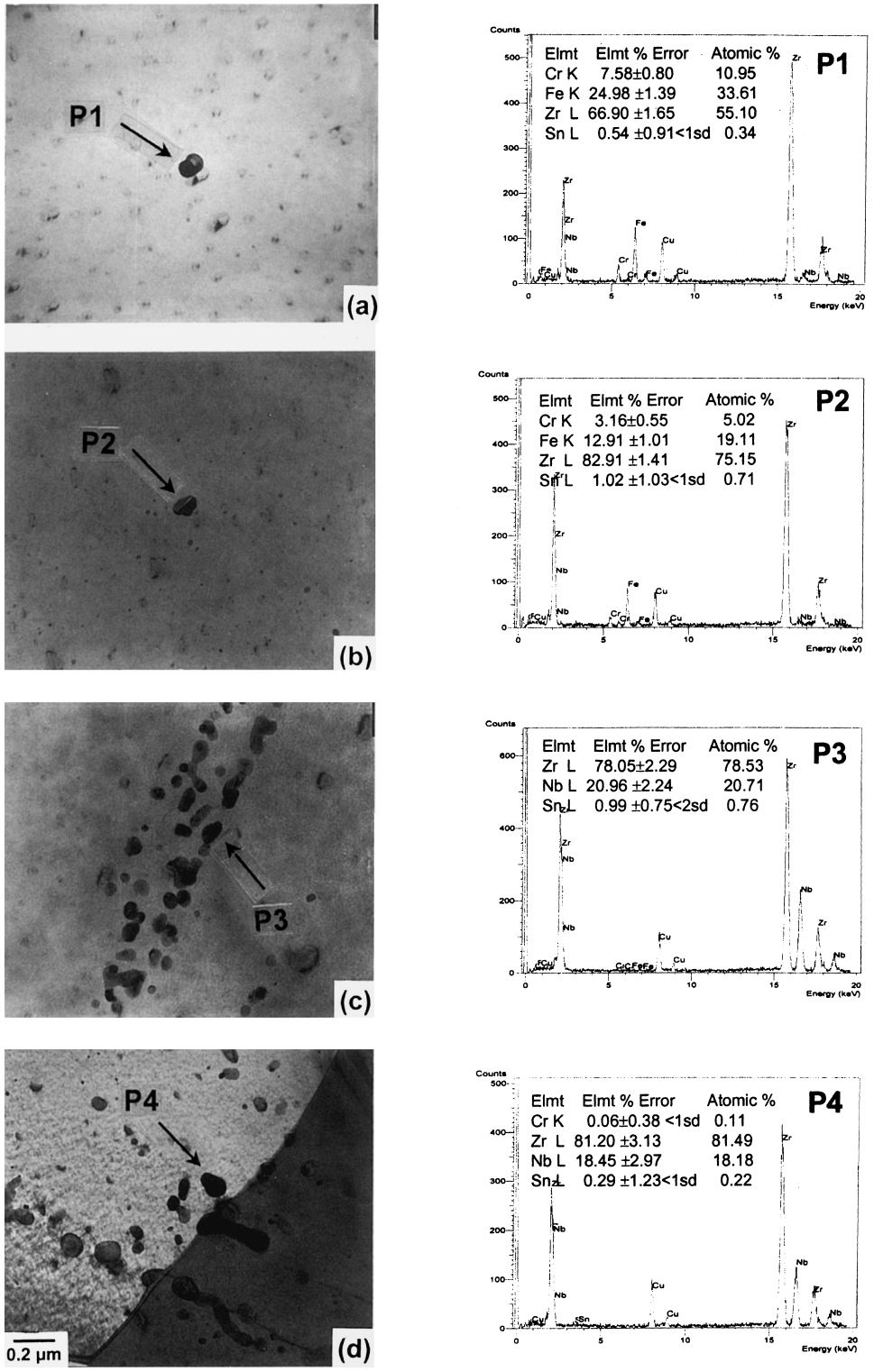

Fig. 8. TEM/EDX analysis of intermetallic precipitates in Zr–0.8Sn–*Y*Nb alloys: (a) $Y = 0.2$; (b) $Y = 0.4$; (c) $Y = 0.8$; (d) $Y = 1.0$.

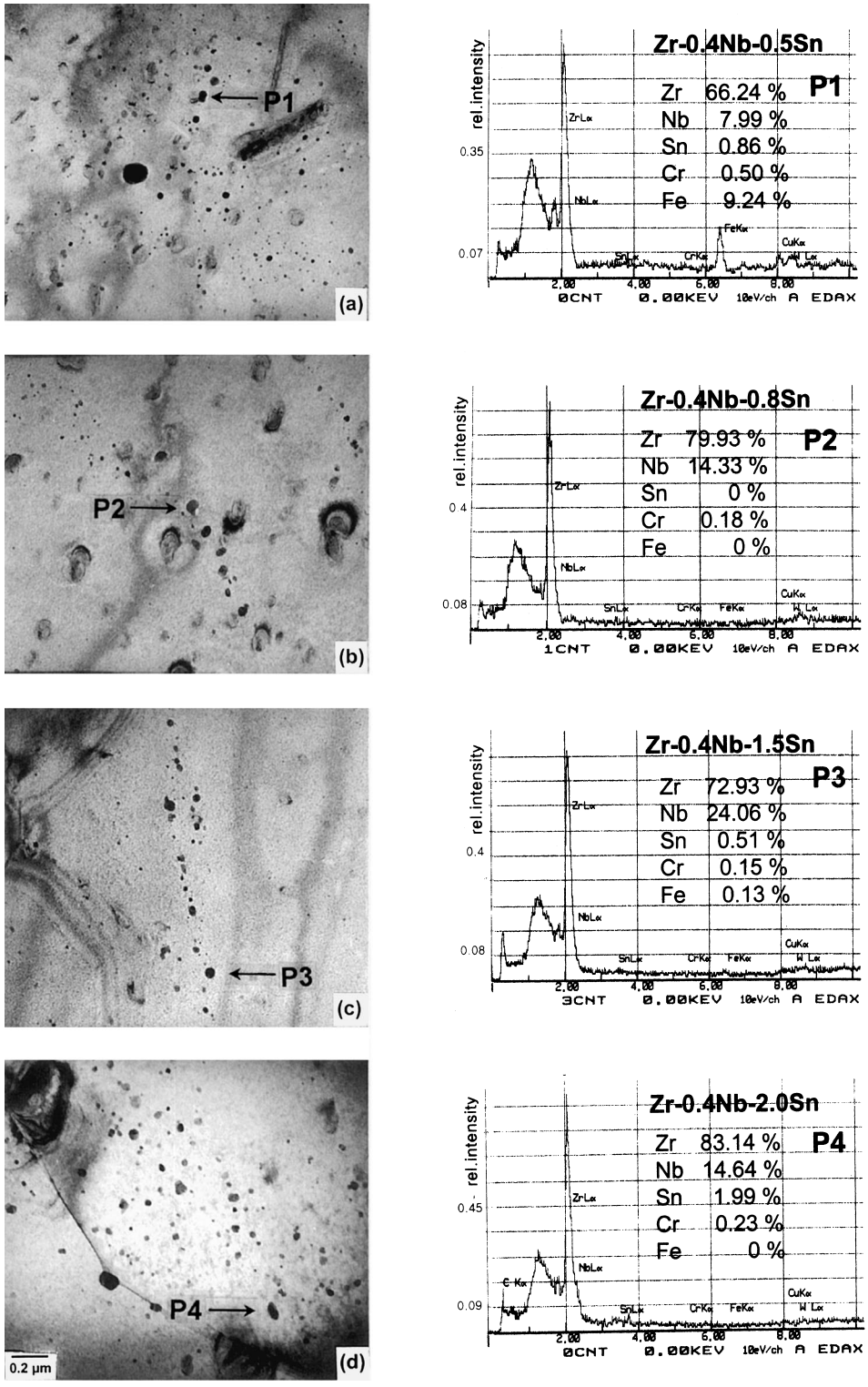

Fig. 9. TEM/EDX analysis of intermetallic precipitates in Zr–0.4Nb–*X*Sn alloys: (a) $X = 0.5$; (b) $X = 0.8$; (c) $X = 1.5$; (d) $X = 2.0$.

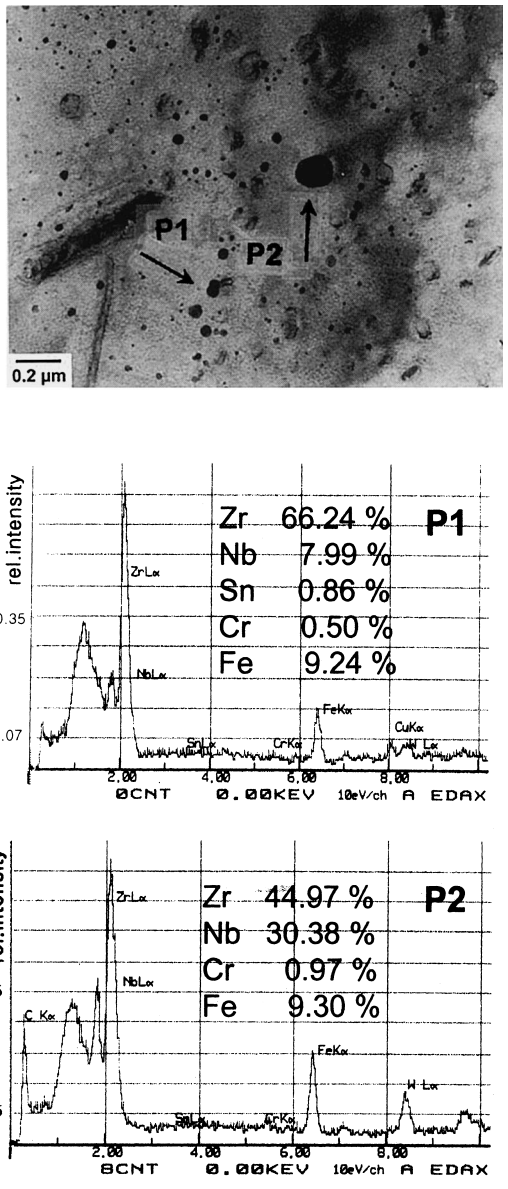

Fig. 10. TEM/EDX analysis of intermetallic precipitates in Zr–0.4Nb–0.5Sn alloys.

solubility limit of Nb (~0.5 %) in the binary may still be valid in this ternary system. The EDX analysis reveals that the precipitates are two types of intermetallic compounds, Zr(Fe,Cr)-type and Zr_4Nb-type. These figures show that the precipitates apparently have a tendency to decompose, grow, and align into a line with round or elliptic shapes.

However, even with the many precipitates formed in the alloy, the reaction rate does not increase much. This means that the formation of precipitates does not affect the hydriding reaction rate. If the precipitates were acting as absorption sites, the rate should have increased abruptly when Nb content exceeded 0.4 wt%. It is believed that Nb has no characteristic effects on hydrogen pick-up or absorption since the Zr–Nb binary system is known to be very resistant to hydriding [10].

In contrast to the precipitates induced by Nb addition, TEM micrographs reveal, unexpectedly, that there are no Sn-precipitates even in the Zr–0.4Nb–1.5Sn and Zr–0.4Nb–2.0Sn alloys (in Fig. 9), which means the shift of the solubility limit of the tin to a higher content above 2.0% in the ternary system. Therefore, the rate change of the hydriding kinetics in the Zr–0.4Nb–*X*Sn alloy system is also irrelevant to the intermetallic precipitates. Instead, the kinetic behavior with a minimum rate at a certain composition (around 1.5 wt%) may be related to the elemental characteristics in the hydrogen pick-up or absorption. It is noticeable that Nb-precipitates are observed in all Zr–0.4Nb–*X*Sn ternary alloys, even though the alloy has Nb content lower than its solubility limit. Compositions of two precipitates in the alloy, P1 (small ppt.) and P2 (large ppt.), are analyzed quantitatively (Fig. 10). It turns out that P1 has 7.99% Nb while P2 has 30.38% Nb. This indicates that the bigger the precipitate grows, the more Nb is concentrated into the precipitate, that is, Nb plays a significant role in the precipitation. As seen in EDX spectra, Nb composition in most precipitates of Zr–0.4Nb–0.5Sn is in the range of 8–30%. Finally, it turns out that there is no strong relationship between the intermetallic precipitates and the hydrogen absorption rate in the Zr–*X*Sn–*Y*Nb alloy system.

4. Conclusions

Effects of Sn and Nb on the massive hydriding kinetics of Zr–0.4Nb–*X*Sn ($X = 0.5, 0.8, 1.5, 2.0$) and Zr–0.8Sn–*Y*Nb ($Y = 0.2, 0.4, 0.8, 1.0$) ternary alloys are examined at 400°C under atmospheric pressure by in situ thermo-gravimetric measurements and TEM/EDX analysis. From the experimental results, the following conclusions are drawn.

1. Hydriding kinetics of the two ternary alloys, Zr–0.4Nb–*X*Sn and Zr–0.8Sn–*Y*Nb, follows a linear rate law after the incubation time.
2. The reaction rate decreases with increasing Sn content up to 1.5%, and then sharply increases in the case of Zr–0.4Nb–*X*Sn alloys. On the other hand, it steadily increases with Nb content in the case of Zr–0.8 Sn–*Y*Nb alloys.
3. The kinetics does not seem to be affected by the recrystallized grain size in Zr–0.4Nb–*X*Sn alloys, but influenced in cases of Zr–0.8Sn–*Y*Nb alloys.
4. TEM/EDX analysis shows that there is no strong relationship between the intermetallic precipitation and the rate of the hydrogen absorption in the Zr–*X*Sn–*Y*Nb alloy system.

5. TEM/EDX analysis also demonstrates that the solubility limit of Sn in the Zr–0.4Nb–*X*Sn ternary system becomes higher than that in the Zr–Sn binary system while the Nb solubility limit in the Zr–0.8Sn–*Y*Nb system remains unchanged. In addition, it is revealed that Nb plays a significant role in the formation of intermetallic precipitates in the Zr–*X*Sn–*Y*Nb ternary alloys even when the concentrations of the two alloying elements are low.
6. Optimized compositions in the Zr–*X*Sn–*Y*Nb ternary alloy are suggested to be about 1.5% Sn and as low Nb as possible in order to minimize the hydrogen uptake.

Acknowledgements

We would like to thank Dr Y.H. Jeong and his colleagues at Korea Atomic Energy Research Institute for supplying the alloys for our experiments. Valuable discussion with them was also much appreciated.

References

[1] A.M. Garde, in: Proceedings of the Ninth International Symposium on Zirconium in the Nuclear Industry, ASTM STP 1132, 1991, p. 556.
[2] M. Blat, D. Noel, in: Proceedings of the 11th International Symposium on Zirconium in the Nuclear Industry, ASTM STP 1295, 1996, p. 319.
[3] M. Blat, J. Bourgoin, in: Proceedings of the International Topical Meeting on LWR Fuel Preformance, Portland, Oregon, USA, 2–6 March 1997, 250.
[4] G. Meyer, M. Kobrinsky, J.P. Abriata, J.C. Bolcich, J. Nucl. Mater. 229 (1996) 48.
[5] Y. Kim, S. Kim, J. Nucl. Mater. 270 (1999) 147.
[6] E.A. Gulbransen, K.F. Andrew, J. Met. 185 (1949) 515.
[7] J. Belle, B.B. Cleland, M.W. Mallett, J. Electrochem. Soc. 101 (1954) 211.
[8] S. Naito, J. Chem. Phys. 79 (1983) 3113.
[9] K. Une, J. Less-Common Met. 57 (1978) 93.
[10] A.M. Garde, S.R. Pati, M.A. Krammen, G.P. Smith, R.K. Endter, in: Proceedings of the 10th International Symposium on Zirconium in the Nuclear Industry, ASTM STP 1245, 1994, p. 760.
[11] Y.H. Jeong et al., KAERI/RR-1668, 1996.
[12] V.F. Urbanic, P.K. Chan, D Khatamian, O.T. Woo, in: Proceedings of the 10th International Symposium on Zirconium in the Nuclear Industry, ASTM STP 1245, 1994, p. 116.
[13] L.F.P. Van Swam, S.H. Shann, in: Proceedings of the Ninth International Symposium on Zirconium in the Nuclear Industry, ASTM STP 1132, 1991, p. 758.
[14] B. Cheng, P.M. Gilmore, H.H. Klepfer, in: Proceedings of the 11th International Symposium on Zirconium in the Nuclear Industry, ASTM STP 1295, 1996, p. 137.
[15] F. Garzarolli, E. Steinberg, H.G. Weidinger, in: Proceedings of the Eighth International Symposium on Zirconium in the Nuclear Industry, ASTM STP 1023, 1989, p. 202.
[16] C.E.L. Hunt, P. Niessen, J. Nucl. Mater. 38 (1971) 17.
[17] D. Charquet, R. Hahn, E. Ortlieb, J.F. Gros, J.P. Wadier, in: Proceedings of the Eighth International Symposium on Zirconium in the Nuclear Industry, ASTM STP 1023, 1989, p. 405.
[18] G.P. Sabol, G.R. Kilp, M.G. Balfour, E. Roberts, in: Proceedings of the Eighth International Symposium on Zirconium in the Nuclear Industry, ASTM STP 1023, 1989, p. 227.
[19] B. Wadman, Z. Lai, H.O. Andren, A.L. Nyström, P. Ruding, H. Pettersson, in: Proceedings of the 10th International Symposium on Zirconium in the Nuclear Industry, ASTM STP 1245, 1994, p. 579.
[20] J. Godlewski, in: Proceedings of the 10th International Symposium on Zirconium in the Nuclear Industry, ASTM STP 1245, 1994, p. 663.